LABORATORI NAZIONALI DI FRASCATI
SIS-Pubblicazioni

**LNF-07/27 (P)**
26 November 2007

# STERILE NEUTRINOS AT THE CNGS

A. Donini[1], M. Maltoni[1], D. Meloni[2] P. Migliozzi[3], F. Terranova[4]
[1)] *I.F.T. and Dep. Física Teórica, U.A.M., Madrid, Spain*
[2)] *I.N.F.N., Sezione di Roma I and Dip. Fisica, Univ. Roma "La Sapienza", Rome, Italy*
[3)] *I.N.F.N., Sez. di Napoli, Napoli, Italy*
[4)] *I.N.F.N., Laboratori Nazionali di Frascati, Frascati (Rome), Italy*

**Abstract**

We study the potential of the CNGS beam in constraining the parameter space of a model with one sterile neutrino separated from three active ones by an $\mathcal{O}(\mathrm{eV}^2)$ mass-squared difference, $\Delta m^2_{\mathrm{SBL}}$. We perform our analysis using the OPERA detector as a reference (our analysis can be upgraded including a detailed simulation of the ICARUS detector). We point out that the channel with the largest potential to constrain the sterile neutrino parameter space at the CNGS beam is $\nu_\mu \to \nu_\tau$. The reason for that is twofold: first, the active-sterile mixing angle that governs this oscillation is the less constrained by present experiments; second, this is the signal for which both OPERA and ICARUS have been designed, and thus benefits from an extremely low background. In our analysis we also took into account $\nu_\mu \to \nu_e$ oscillations. We find that the CNGS potential to look for sterile neutrinos is limited with nominal intensity of the beam, but it is significantly enhanced with a factor 2 to 10 increase in the neutrino flux. Data from both channels allow us, in this case, to constrain further the four-neutrino model parameter space. Our results hold for any value of $\Delta m^2_{\mathrm{SBL}} \gtrsim 0.1$ eV$^2$, *i.e.* when oscillations driven by this mass-squared difference are averaged. We have also checked that the bound on $\theta_{13}$ that can be put at the CNGS is not affected by the possible existence of sterile neutrinos.

PACS: 14.60.Pq, 14.60.Lm

*Submitted to JHEP*

## 1 Introduction

The results of solar [1–6], atmospheric [7,8], reactor [9–12] and accelerator [13–15] neutrino experiments show that flavour mixing occurs not only in the hadronic sector, as it has been known for long, but in the leptonic sector as well. The full understanding of the leptonic mixing matrix constitutes, together with the discrimination of the Dirac/Majorana character of neutrinos and with the measurement of their absolute mass scale, the main goal of neutrino physics for the next decade.

The experimental results point to two very distinct mass-squared differences, $\Delta m^2_{\rm sol} \approx 7.9 \times 10^{-5}$ eV$^2$ and $|\Delta m^2_{\rm atm}| \approx 2.4 \times 10^{-3}$ eV$^2$. On the other hand, only two out of the four parameters of the three-family leptonic mixing matrix $U_{\rm PMNS}$ [16–19] are known: $\theta_{12} \approx 34^\circ$ and $\theta_{23} \approx 43^\circ$ [20]. The other two parameters, $\theta_{13}$ and $\delta$, are still unknown: for the mixing angle $\theta_{13}$ direct searches at reactors [9–11] and three-family global analysis of the experimental data give the upper bound $\theta_{13} \leq 11.5^\circ$, whereas for the leptonic CP-violating phase $\delta$ we have no information whatsoever (see, however, Ref. [20]).

The LSND data [21–23], on the other hand, would indicate a $\bar\nu_\mu \to \bar\nu_e$ oscillation with a third neutrino mass-squared difference: $\Delta m^2_{\rm LSND} \sim 0.3{-}6$ eV$^2$, about two orders of magnitude larger than $\Delta m^2_{\rm atm}$. Given the strong hierarchy among the solar, atmospheric and LSND mass-squared splittings, $\Delta m^2_{\rm sol} \ll \Delta m^2_{\rm atm} \ll \Delta m^2_{\rm SBL}$, it is not possible to explain all these data with just three massive neutrinos, as it has been shown with detailed calculations in Ref. [24]. A necessary condition to explain the whole ensemble of data in terms of neutrino oscillations is therefore the introduction of *at least* a fourth light neutrino state. This new light neutrino must be an electroweak singlet [18] in order to comply with the strong bounds on the $Z^0$ invisible decay width [25,26]. For this reason, the LSND signal has often been considered as an evidence of the existence of a sterile neutrino.

In recent years, global analyses of solar, atmospheric, short-baseline [27–30] experiments and LSND data have been performed to establish whether four-neutrino models can really reconcile the data and solve the puzzle [31–38]. The point is that providing a suitable mass-squared difference to each class of experiments is not enough: it is also necessary to show that the intrinsic structure of the neutrino mixing matrix is compatible with all the data. This turned out to be very hard to accomplish. In Ref. [39] it was shown that four-neutrino models were only marginally allowed, with best fit around $\Delta m^2_{\rm LSND} \simeq 1$ eV$^2$ and $\sin^2 2\theta_{\rm LSND} \simeq 10^{-3}$. Generically speaking, the global analysis indicated that a single sterile neutrino state was not enough to reconcile LSND with the other experiments. For this reason, to improve the statistical compatibility between the

LSND results and the rest of the oscillation data, models with two sterile neutrino states have been tested (see, for example, Ref. [40] and references therein). Although a slightly better global fit was achieved, a strong tension between the LSND data and the results from atmospheric and short-baseline experiments was still present.

So far, the LSND signal has not been confirmed by any other experiment [41]. It is therefore possible that the LSND anomaly arises from some some yet unknown problem in the data set itself. To close the issue, the MiniBooNE collaboration [42] at FermiLab has recently performed a search for $\nu_\mu \to \nu_e$ appearance with a baseline of 540 m and a mean neutrino energy of about 700 MeV. The primary purpose of this experiment was to test the evidence for $\bar{\nu}_\mu \to \bar{\nu}_e$ oscillation observed at LSND with a very similar $L/E$ range. No evidence of the expected signal has been found, hence ruling out once and for all the four-neutrino interpretation of the LSND anomaly. However, MiniBooNE data are themselves not conclusive: although no evidence for $\nu_\mu \to \nu_e$ oscillation has been reported in the spectrum region compatible with LSND results, an unexplained excess has been observed for lower energy neutrinos. Furthermore, within a five-neutrino model this excess can be easily explained, and even reconciled with LSND and all the other *appearance* experiments [43]. On the other hand, a post-MiniBooNE global analysis including also *disappearance* data show that five-neutrino models suffer from the same problems as four-neutrino schemes, and in particular they are now only marginally allowed – a situation very similar to that of four-neutrino models before MiniBooNE data. Adding a third sterile neutrino[1] does not help [43], and in general global analyses seem to indicate that sterile neutrinos alone are not enough to reconcile all the data. Models with sterile neutrinos and exotic physics have been therefore proposed (see, for example, Ref. [46]).

In summary, the present experimental situation is still confused. It is therefore worthwile to understand if, aside of MiniBooNE, new neutrino experiments currently running or under construction can investigate the existence of sterile neutrinos separated from the active ones by $\mathcal{O}(\mathrm{eV}^2)$ mass-squared differences. In this paper we explore in detail the capability of the CNGS beam to perform this search. For definiteness we focus on the simplest case with only one extra sterile neutrino. Note that this model is perfectly viable once the LSND result is dropped, as it contains as a limiting case the usual three-neutrino scenario. Furthermore, it is easily generalizable by adding new sterile neutrino states, and it can be used as a basis for models with extra "sterile" states strongly decoupled from active neutrinos (such as in extra-dimensions models with a right-handed

[1] A quite interesting scenario is, in our opinion, that in which three right-handed Majorana neutrinos are added to the three weakly-interacting ones. If the Majorana mass term $M$ is $\mathcal{O}(\mathrm{eV})$, (3+3) light Majorana neutrinos are present at low-energy [44,45].

neutrino in the bulk [47]).

The CNGS beam [48] has been built to test the (supposedly) dominant oscillation in atmospheric neutrino data, $\nu_\mu \to \nu_\tau$. In order to make possible $\tau$ production through CC interactions, the mean neutrino energy, $\langle E_\nu \rangle = 17$ GeV, is much above the atmospheric oscillation peak for the CERN to Gran Sasso baseline, $L = 732$ Km. Two detectors are illuminated by the CNGS beam: OPERA (see Ref. [49] and refs. therein) will start data taking with the lead-emulsion target in 2007; ICARUS-T600 (see Ref. [50] and refs. therein) will start operating in 2008. Both detectors have been especially designed to look for $\tau$'s produced through $\nu_\mu \to \nu_\tau$ oscillation and to minimize the corresponding backgrounds. The expected number of $\tau$ events after signal selection in an experiment such as OPERA (after five years of data taking with nominal CNGS luminosity) is $\mathcal{O}(10)$ events with $\mathcal{O}(1)$ background event.

At the CNGS distance and energy, neutrino oscillations mediated by an $\mathcal{O}(\mathrm{eV}^2)$ mass difference will appear as a constant term in the oscillation probability. In four-neutrino models, fluctuations induced by this term over the atmospheric $\nu_\mu \to \nu_\tau$ oscillation can be as large as 100% for specific points of the allowed parameter space. This is due to the fact that the leading angle for this oscillation is the less constrained one. The $\nu_\mu \to \nu_\tau$ channel, therefore, is extremely promising as a "sterile neutrino" smoking gun, as it has been commented elsewhere (see, for example, Refs. [51,52] and refs. therein). To test the model we will also make use of the $\nu_\mu \to \nu_e$ channel. Notice that the background to this signal coming from $\tau \to e$ decay is modified in four-neutrino models with respect to standard three-family oscillations. In fact, since $\nu_\mu \to \nu_\tau$ oscillations are depleted by active-sterile mixing with respect to standard ones, the $\tau \to e$ background to $\nu_\mu \to \nu_e$ oscillations gets depleted, too. A combined analysis of the two channels in four-neutrino models at the OPERA detector has been performed, taking into account properly all of the backgrounds. We stress, however, that the same analysis could be performed at ICARUS, as well. The previous considerations hold for any facility operating well beyond the kinematical threshold for $\tau$ production.

In the specific case of the CNGS beam, the limited flux implies a modest improvement in the parameter space exclusion, see Sec. 6. An increase in the exposure of such facilities, however, would permit to improve the present bounds on the parameters of four-neutrino models and, in particular, to constrain the leading angle in $\nu_\mu \to \nu_\tau$ oscillations at the level of the other mixing parameters.

The paper is organized as follows. In Sec. 2 we briefly review the main features of four-neutrino models and we introduce our parametrization of the mixing matrix. In

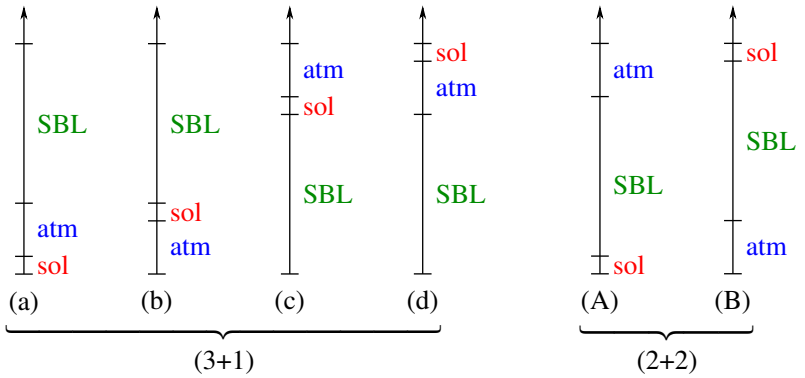


Figure 1: *The two classes of four–neutrino mass spectra, (3+1) and (2+2).*

Sec. 3 we compute the vacuum oscillation probabilities in the atmospheric regime and we review the present bounds on the active-sterile mixing angles. In Sec. 4 we recall the most relevant parameters of CNGS. In Sec. 5 we study theoretically the expectations of the $\nu_\mu \to \nu_\tau$ and $\nu_\mu \to \nu_e$ channels at the CNGS. In Sec. 6 we present our results using these channels at the OPERA detector and the CNGS beam. Finally, in Sec. 7 we draw our conclusions.

## 2 Four neutrino mass schemes

In four-neutrino models, one extra sterile state is added to the three weakly interacting ones. The relation between the flavor and the mass eigenstates is then described by a $4 \times 4$ unitary matrix $U$, which generalizes the usual $3 \times 3$ matrix $U_{\rm PMNS}$ [16–19]. As stated in the introduction, in this work we only consider the case when the fourth mass eigenstate is separated by the other three by an $\mathcal{O}(\mathrm{eV}^2)$ mass-squared gap. There are six possible four-neutrino schemes, shown in Fig. 1, that can accommodate the results from solar and atmospheric neutrino experiments and contain a third much larger $\Delta m^2$. They can be divided in two classes: (3+1) and (2+2). In the (3+1) schemes, there is a group of three close-by neutrino masses that is separated from the fourth one by the larger gap. In (2+2) schemes, there are two pairs of close masses separated by the large gap. While different schemes within the same class are presently indistinguishable, schemes belonging to different classes lead to very different phenomenological scenarios.

A characteristic feature of (2+2) schemes is that the extra sterile state cannot be simultaneously decoupled from *both* solar and atmospheric oscillations. To understand

why, let us define

$$\eta_s = \sum_{i \in \text{sol}} |U_{si}|^2 \qquad \text{and} \qquad c_s = \sum_{j \in \text{atm}} |U_{sj}|^2 \tag{1}$$

where the sums in $i$ and $j$ run over mass eigenstates involved in solar and atmospheric neutrino oscillations, respectively. Clearly, the quantities $\eta_s$ and $c_s$ describe the fraction of sterile neutrino relevant for each class of experiment. Results from atmospheric and solar neutrino data imply that in both kind of experiments oscillation takes place mainly between active neutrinos. Specifically, from Fig. 46 of Ref. [20] we get $\eta_s \leq 0.30$ and $c_s \leq 0.36$ at the $3\sigma$ level. However, in (2+2) schemes unitarity implies $\eta_s + c_s = 1$, as can be easily understood by looking at Fig. 1. These models are therefore ruled out at a very high confidence level [53], and in the rest of this work we will not consider them anymore.

On the other hand, (3+1) schemes are not affected by this problem. Although the experimental bounds on $\eta_s$ and $c_s$ quoted above still hold, the condition $\eta_s + c_s = 1$ no longer applies. For what concerns neutrino oscillations, (3+1) models are essentially unfalsifiable, since they reduce to the conventional three-neutrino scenario when the mixing between active and sterile states are small enough.

The mixing matrix $U$ can be conveniently parametrized in terms of six independent rotation angles $\theta_{ij}$ and three (if neutrinos are Dirac fermions) or six (if neutrinos are Majorana fermions) phases $\delta_i$. In oscillation experiments, only the so-called "Dirac phases" can be measured, the effect of the "Majorana phases" being suppressed by factors of $m_\nu/E_\nu$. The Majorana or Dirac nature of neutrinos can thus be tested only in $\Delta L = 2$ transitions such as neutrino-less double $\beta$-decay [54] or lepton number violating decays [25]. In the following analysis, with no loss in generality, we will restrict ourselves to the case of 4 Dirac-type neutrinos only.

A generic rotation in a four-dimensional space can be obtained by performing six different rotations along the Euler axes. Since the ordering of the rotation matrices $R_{ij}$ (where $ij$ refers to the plane in which the rotation takes place) is arbitrary, plenty of different parametrizations of the mixing matrix $U$ are allowed. The large parameter space (6 angles and 3 phases, to be compared with the standard three-family mixing case of 3 angles and 1 phase) is however reduced to a subspace whenever some of the mass differences become negligible. If the eigenstates $i$ and $j$ are degenerate, rotations in the $ij$-plane become unphysical and the corresponding mixing angle should drop from oscillation probabilities. If the matrix $R_{ij}$ is the rightmost one the angle $\theta_{ij}$ automatically disappears, since the matrix commutes with the vacuum hamiltonian. The parameter space gets therefore reduced to the physical angles and phases. If a different ordering of

the rotation matrices is taken, no angle explicitly disappears from the oscillation formulas, but the physical parameter space is still smaller than the original one. In this case, a parameter redefinition is needed to reduce the parameter space to the observable sector. In Refs. [55,56] it was shown how the one-mass dominance ($\Delta_{\rm sol} \to 0$ and $\Delta_{\rm atm} \to 0$, where $\Delta = \Delta m^2 L/4E$ [57]) and two-mass dominance ($\Delta_{\rm sol} \to 0$) approximations can be implemented in a transparent way (in the sense that only the physical parameters appear in oscillation probabilities) using a parametrization in which rotations are performed in the planes corresponding to smallest mass difference first:

$$U_{\rm SBL} = R_{14}(\theta_{14})\; R_{24}(\theta_{24})\; R_{34}(\theta_{34})\; R_{23}(\theta_{23},\, \delta_3)\; R_{13}(\theta_{13},\, \delta_2)\; R_{12}(\theta_{12},\, \delta_1)\,. \qquad (2)$$

This parametrization was shown to be particularly useful when maximizing oscillations driven by a $\mathcal{O}(\mathrm{eV}^2)$ mass difference. The analytical expressions for the oscillation probabilities in the (3+1) model in the one-mass dominance approximation in this parametrization have been presented in Ref. [51].

In this paper, however, we are interested in a totally different regime: the "atmospheric regime", with oscillations driven by the atmospheric mass difference, $\Delta m^2_{\rm atm} L/E \sim \pi/2$. We will then make use of the following parametrization, adopted in Ref. [43]:

$$U_{\rm atm} = R_{34}(\theta_{34})\; R_{24}(\theta_{24})\; R_{23}(\theta_{23},\, \delta_3)\; R_{14}(\theta_{14})\; R_{13}(\theta_{13},\, \delta_2)\; R_{12}(\theta_{12},\, \delta_1)\,. \qquad (3)$$

It is convenient to put phases in $R_{12}$ (so that it automatically drops in the two-mass dominance regime) and $R_{13}$ (so that it reduces to the "standard" three-family Dirac phase when sterile neutrinos are decoupled). The third phase can be put anywhere; we will place it in $R_{23}$. Note that in the one-mass dominance regime all the phases disappear from the oscillation probabilities.

## 3 Oscillation probabilities and allowed parameter space

Let us first consider $\nu_e$ disappearance at $L/E$ such that $\Delta_{\rm sol}$ can be safely neglected with respect to $\Delta_{\rm atm}$ and $\Delta_{\rm SBL}$. We get for this probability in vacuum:

$$P_{ee} = 1 - \sin^2 2\theta_{14} \sin^2 \frac{\Delta_{\rm SBL} L}{2} - c_{14}^4 \sin^2 2\theta_{13} \sin^2 \frac{\Delta_{\rm atm} L}{2}\,, \qquad (4)$$

where $c_{ij} = \cos\theta_{ij}$ and $s_{ij} = \sin\theta_{ij}$. It is clear from Eq. (4) that reactor experiments such as Bugey and Chooz can put stringent bounds to $\theta_{13}$ and $\theta_{14}$, in this parametrization. This is depicted in Fig. 2(left), where 90%, 95%, 99% and $3\sigma$ CL contours in the $(\theta_{13} - \theta_{14})$-plane are shown for $\Delta_{\rm sol} \to 0$ and $\Delta m^2_{\rm atm} = 2.4 \times 10^{-3}$ eV$^2$. The third mass difference,

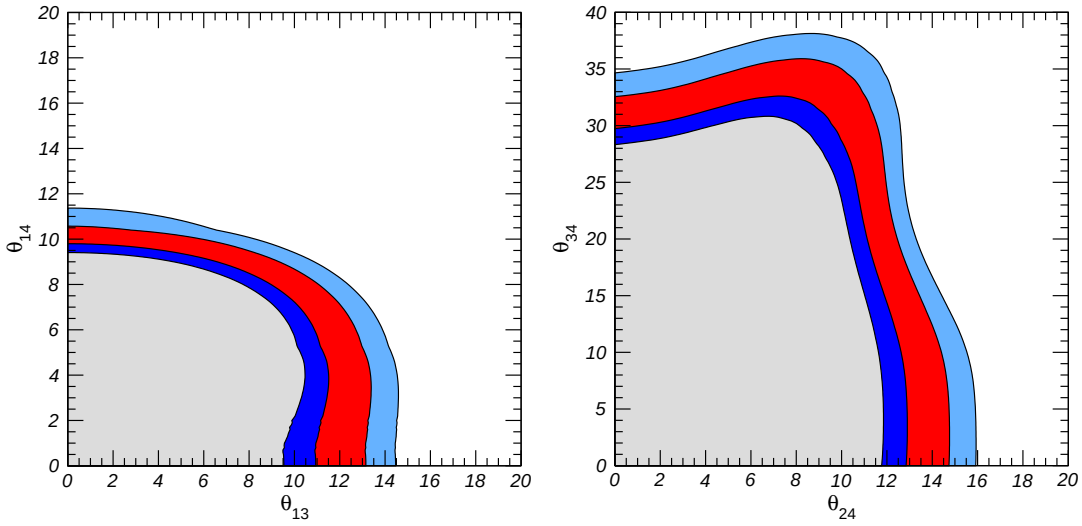


Figure 2: *Allowed regions at 90%, 95%, 99% and 3$\sigma$ CL in the $(\theta_{13},\, \theta_{14})$ plane (left) and in the $(\theta_{24},\, \theta_{34})$ plane (right) from the results of present atmospheric, reactor and LBL neutrino experiments. The undisplayed parameters $\theta_{23}$ and $\delta_3$ are marginalized.*

$\Delta m^2_{\rm SBL}$, is free to vary above $0.1$ eV$^2$. Notice that the $\nu_e$ disappearance probability does not depend on $\theta_{23}, \theta_{24}$ and $\theta_{34}$. It can be clearly seen that the three-family Chooz bound on $\theta_{13}$ is slightly modulated by $\theta_{14}$. Both angles, however, cannot be much larger than $10^\circ$. We will therefore expand in these two parameters to deduce the other relevant oscillation probabilities.

At the CNGS beam atmospheric oscillations are large, solar oscillations can be neglected and $\mathcal{O}(\mathrm{eV}^2)$ oscillations are extremely fast and can be averaged. It is useful to write down the oscillation probability (in vacuum) at typical atmospheric $L/E$, in the approximation $\Delta_{\rm sol} \to 0$, $\Delta_{\rm SBL} \to \infty$. In this regime:

$$\begin{aligned} P(\nu_\alpha \to \nu_\beta) = \delta_{\alpha\beta} &- 4\Re\left[U_{\alpha3}U^\star_{\beta3}\left(\delta_{\alpha\beta} - U^\star_{\alpha3}U_{\beta3} - U^\star_{\alpha4}U_{\beta4}\right)\right]\sin^2\frac{\Delta_{23}L}{2} \\ &- 2\Re\left[\delta_{\alpha\beta}U_{\alpha4}U^\star_{\beta4} - |U_{\alpha4}|^2|U_{\beta4}|^2\right] \pm 2\Im\left[U_{\alpha3}U^\star_{\beta3}U^\star_{\alpha4}U_{\beta4}\right]\sin\Delta_{23}L\,, \end{aligned} \tag{5}$$

where $+$ stands for neutrinos and $-$ for antineutrinos, respectively. Up to second order in $\theta_{13}$ and $\theta_{14}$ we get for the $\nu_\mu$ disappearance oscillation probability:

$$\begin{aligned} P_{\mu\mu} = 1 - 2c^2_{14}s^2_{24}(1 - c^2_{14}s^2_{24}) - 4\Big\{ & s^2_{23}c^2_{24}\left[c^2_{24}(c^2_{23} - s^2_{13}) - s^2_{14}s^2_{24}\right] \\ & - 2c^3_{24}s_{23}(1 - 2s^2_{23})s_{13}s_{14}s_{24}\cos(\delta_2 - \delta_3)\Big\}\sin^2\frac{\Delta_{\rm atm}L}{2}\,. \end{aligned} \tag{6}$$

A "negative" result in an atmospheric $L/E$ $\nu_\mu$ disappearance experiment (such as, for example, K2K), in which $\nu_\mu$ oscillations can be very well fitted in terms of three-family

oscillations, will put a stringent bound on the mixing angle $\theta_{24}$. The bound from such experiments on $\theta_{24}$ can be seen in Fig. 2(right), where 90%, 95%, 99% and $3\sigma$ CL contours in the $(\theta_{24} - \theta_{34})$-plane are shown for $\Delta_{\rm sol} \to 0$ and $\Delta m^2_{\rm atm} = 2.4 \times 10^{-3}$ eV$^2$. The third mass difference, $\Delta m^2_{\rm SBL}$, is free to vary above $0.1$ eV$^2$. The mixing angles not shown have been fixed to: $\theta_{23} = 45^\circ$; $\theta_{13} = \theta_{14} = 0$ (in this hypothesis, $P_{\mu\mu}$ does not depend on phases). Notice that the $\nu_\mu$ disappearance probability does not depend on $\theta_{34}$.

From the figure, we can see that $\theta_{24}$ cannot be much larger than $10^\circ$, either. We will consider, therefore, the three mixing angles $\theta_{13}, \theta_{14}$ and $\theta_{24}$ being of the same order and expand in powers of the three. At second order in $\theta_{13}, \theta_{14}$ and $\theta_{24}$, we get:

$$P_{\mu\mu} = 1 - 2s^2_{24} - 4s^2_{23}\left[c^2_{23}(1 - 2s^2_{24}) - s^2_{13}\right]\sin^2\frac{\Delta_{\rm atm}L}{2}\,. \tag{7}$$

Since both $\nu_e$ and $\nu_\mu$ disappearance do not depend on $\theta_{34}$, we should ask which measurements give the upper bound to this angle that can be observed in Fig. 2(right). This is indeed a result of indirect searches for $\nu_\mu \to \nu_s$ conversion in atmospheric experiments, using the different interaction with matter of active and sterile neutrinos. This can be understood from the (vacuum) $\nu_\mu \to \nu_s$ oscillation probability at atmospheric $L/E$ for which, at second order in $\theta_{13}, \theta_{14}$ and $\theta_{24}$, we get:

$$\begin{aligned} P_{\mu s} = {} & 2c^2_{34}s^2_{24} + \Big\{ \sin^2 2\theta_{23}(c^4_{13}c^2_{24}s^2_{34} - c^2_{34}s^2_{24}) \\ & + 2c_{34}\sin 2\theta_{23}s_{34}\left[s_{24}(1 - 2s^2_{23})\cos\delta_3 + 2s_{23}s_{13}s_{14}\cos\delta_2\right]\Big\}\sin^2\frac{\Delta_{\rm atm}L}{2} \\ & \pm c_{34}\sin 2\theta_{23}s_{24}s_{34}\sin\delta_3\sin\Delta_{\rm atm}L\,. \end{aligned} \tag{8}$$

As it can be seen, the bound on $\theta_{34}$ arises from a measurement of spectral distortion (*i.e.*, from the "atmospheric" term proportional to $\sin^2\Delta_{\rm atm}L/2$). On the other hand, bounds on $\theta_{13}, \theta_{14}$ and $\theta_{24}$ are mainly drawn by a flux normalization measurement. As a consequence, the bound on $\theta_{34}$ that we can draw by non-observation of $\nu_\mu \to \nu_s$ oscillation in atmospheric experiments is less stringent than those we have shown before. For this reason, $\theta_{34}$ can be somewhat larger than $\theta_{13}, \theta_{14}$ and $\theta_{24}$, but still bounded to be below $40^\circ$. In the following, we will expand in powers of the four mixing angles $\theta_{13}, \theta_{14}, \theta_{24}$ and $\theta_{34}$, that will be considered to be comparably small.

Up to fourth-order in $\theta_{13}, \theta_{14}, \theta_{24}$ and $\theta_{34}$, the $\nu_\mu \to \nu_e$ appearance probability in the atmospheric regime is:

$$\begin{aligned} P_{\mu e} = {} & 4\left\{s^2_{23}s^2_{13}[1 - s^2_{13} - s^2_{14} - s^2_{24}] + s_{23}s_{13}s_{14}s_{24}\cos(\delta_2 - \delta_3)\right\}\sin^2\frac{\Delta_{\rm atm}L}{2} \\ & \pm 2s_{23}s_{13}s_{14}s_{24}\sin(\delta_2 - \delta_3)\sin\Delta_{\rm atm}L + 2s^2_{14}s^2_{24}\,. \end{aligned} \tag{9}$$

Eventually, the $\nu_\mu \to \nu_\tau$ appearance probability up to fourth-order in $\theta_{13}, \theta_{14}, \theta_{24}$ and $\theta_{34}$ in the atmospheric regime is:

$$\begin{aligned} P_{\mu\tau} = {} & 2 s^2_{24} s^2_{34} + \left\{ \sin^2 2\theta_{23} [c^4_{13} c^2_{24} c^2_{34} - s^2_{24} s^2_{34}] \right. \\ & - 4 \sin 2\theta_{23} s_{13} s_{14} [s_{23} s_{34} \cos\delta_2 + c_{23} s_{24} \cos(\delta_2 - \delta_3)] \\ & \left. + 2 \sin 2\theta_{23} s_{24} s_{34} c^2_{13} c^2_{24} c_{34} [c^2_{14} - 2 c^2_{13} s^2_{23}] \cos\delta_3 \right\} \sin^2 \frac{\Delta_{\text{atm}} L}{2} \\ & \mp \sin 2\theta_{23} s_{24} s_{34} c^2_{13} c^2_{14} c^2_{24} c_{34} \sin\delta_3 \sin \Delta_{\text{atm}} L \, . \end{aligned} \tag{10}$$

As it was shown in Refs. [51,52], the $\nu_\mu \to \nu_\tau$ appearance channel is a good place to look for sterile neutrinos. This can be understood as follows: consider the $\nu_\mu \to \nu_\tau$ three-family oscillation probability in the atmospheric regime, up to fourth-order in $\theta_{13}$:

$$P^{3\nu}_{\mu\tau} = P_{\mu\tau}(\theta_{i4} = 0) \simeq c^4_{13} \sin^2 2\theta_{23} \sin^2 \frac{\Delta_{\text{atm}} L}{2} \, . \tag{11}$$

The genuine active-sterile neutrino mixing effects are:

$$\begin{aligned} \Delta P_{\mu\tau} \equiv {} & P_{\mu\tau} - P^{3\nu}_{\mu\tau} \\ = {} & \left\{ -(s^2_{24} + s^2_{34}) \sin^2 2\theta_{23} + 2 \sin 2\theta_{23} (1 - 2 s^2_{13}) s_{24} s_{34} \cos\delta_3 \right\} \sin^2 \frac{\Delta_{\text{atm}} L}{2} \\ & \mp \sin 2\theta_{23} s_{24} s_{34} \sin\delta_3 \sin \Delta_{\text{atm}} L + \ldots \end{aligned} \tag{12}$$

that is second-order in small angles $\theta_{13}, \theta_{14}, \theta_{24}$ and $\theta_{34}$. We would get a similar result for $\nu_\mu$ disappearance, also. On the other hand, computing the corresponding quantity in the $\nu_\mu \to \nu_e$ channel, we get:

$$\begin{aligned} \Delta P_{\mu e} \equiv {} & P_{\mu e} - P_{\mu e}(\theta_{i4} = 0) \\ = {} & s_{23} s_{13} s_{14} s_{24} \cos(\delta_2 - \delta_3) \sin^2 \frac{\Delta_{\text{atm}} L}{2} \\ & \pm 2 s_{23} s_{13} s_{14} s_{24} \sin(\delta_2 - \delta_3) \sin \Delta_{\text{atm}} L + \ldots \end{aligned} \tag{13}$$

that is third-order in the same parameters.

Notice, eventually, that all oscillation probabilities start with an energy-independent term and are, therefore, non-vanishing for $L = 0$, a result of our assumption that $\Delta_{\text{SBL}} \to \infty$.

## 4 The CNGS facility

The CNGS is a conventional neutrino beam in which neutrinos are produced by the decay of secondary pions and kaons, obtained from collisions of 400 GeV protons from the

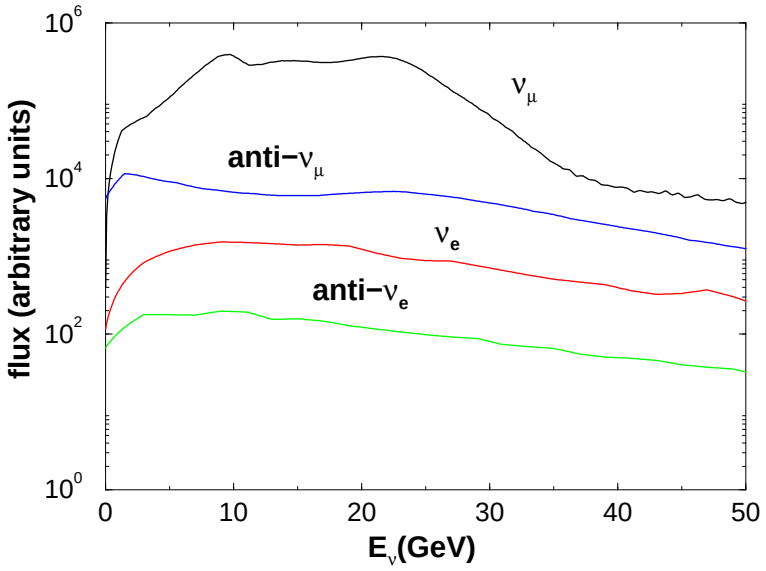


Figure 3: *CNGS neutrino fluxes (in arbitrary units) as a function of the neutrino energy. Both muon and electron neutrino fluxes are illustrated.*

CERN-SPS onto a graphite target. The resulting neutrinos are aimed to the underground Gran Sasso Laboratory (LNGS), located at 730 Km from CERN. This facility provided the first neutrinos in August 2006 [49]. Differently from other long baseline experiments, the neutrinos from CNGS can be exploited to search directly for $\nu_\mu \rightarrow \nu_\tau$ oscillations, since they have a mean energy well beyond the kinematic threshold for $\tau$ production. Moreover, the prompt $\nu_\tau$ contamination (mainly from $D_s$ decays) is negligible. The expected $\nu_e$ contamination is also relatively small compared to the dominant $\nu_\mu$ component, thus allowing for the search of sub-dominant $\nu_\mu \rightarrow \nu_e$ oscillations through an excess of $\nu_e$ CC events.

The energy spectra of the CNGS neutrino beam are shown (in arbitrary units) in Fig. 3 [58]. In the present paper we assume the nominal intensity for the CNGS, corresponding to $4.5 \times 10^{19}$ pot/year.

OPERA has been designed to search for $\tau$ appearance through identification of the $\nu_\tau$ CC interaction on an event-by-event basis. In particular, $\tau$'s are tagged identifying explicitly their decay kink through high resolution nuclear emulsions interleaved with lead sheets. For this detector, we can take advantage of the detailed studies of the $\nu_\mu \rightarrow \nu_\tau$ signal (see Ref. [59]) and of the $\nu_\mu \rightarrow \nu_e$ signal (see Ref. [60]).

The total non-oscillated CC event rates for a 1 Kton lead target with a neutrino flux

| $\nu_\mu$ | $\bar{\nu}_\mu$ | $\nu_e$ | $\bar{\nu}_e$ |
|---|---|---|---|
| 669.0 | 13.7 | 5.9 | 0.3 |

Table 1: *Nominal performance of the CNGS reference beam [58]. The total non-oscillated CC event rates are calculated assuming* $10^{19}$ *pot and 1 Kton lead target mass.*

normalized to $10^{19}$ pot are shown in Tab. 1 and are evaluated according to

$$N = \int \frac{d\phi_{\nu_\alpha}(E)}{dE}\, \sigma_{\nu_\alpha}(E)\, dE\,, \tag{14}$$

in which $\phi_{\nu_\alpha}$ is the flux of the neutrino flavour $\nu_\alpha$ and $\sigma_{\nu_\alpha}$ the corresponding cross section on lead.

## 5 Appearance channels at the CNGS

### 5.1 $\nu_\mu \to \nu_\tau$ oscillations

Since the CNGS experiments have been designed to search for $\nu_\mu \to \nu_\tau$ oscillation in the parameter region indicated by the atmospheric neutrino data, we can take full advantage of them in order to constrain (and, possibly, study) the four-family parameter space.

The number of taus from $\nu_\mu \to \nu_\tau$ oscillations is given by the convolution of the $\nu_\mu$ flux $d\phi_{\nu_\mu}(E)/dE$ with the $\nu_\tau$ charged-current cross-section on lead, $\sigma^{CC}_{\nu_\tau}(E)$, weighted by the $\nu_\mu \to \nu_\tau$ oscillation probability, $P_{\mu\tau}(E)$, times the efficiency for the OPERA detector, $\varepsilon_{\mu\tau}$:

$$N_{\mu\tau} = A \int \frac{d\phi_{\nu_\mu}(E)}{dE}\, P_{\mu\tau}(E) \sigma^{CC}_{\nu_\tau}(E)\, \varepsilon_{\mu\tau}\, dE\,. \tag{15}$$

$A$ is a normalization factor which takes into account the target mass and the normalization of the $\nu_\mu$ flux in physical units. Specializing our analysis for the OPERA detector, we have considered an overall efficiency $\varepsilon_{\mu\tau} \sim 13\%$, [59]. This efficiency takes into account that OPERA is able to exploit several decay modes of the final state $\tau$, using both so-called short and long decays.

The dominant sources of background for the $\nu_\mu \to \nu_\tau$ signal are charm decays and hadronic reinteractions. Both of them only depend on the total neutrino flux and not on the oscillation probabilities. The OPERA experiment at the CNGS beam has been designed precisely to measure this channel, and thus the corresponding backgrounds are extremely low.

In Tab. 2 we report the expected number of $\tau$ events in the OPERA detector, according to Eq. (15), for different values of $\theta_{13}, \theta_{14}, \theta_{24}$ and $\theta_{34}$. Input points have been chosen

| $(\theta_{13};\theta_{14};\theta_{24};\theta_{34})$ | $N_\tau$ | background | $(\theta_{13};\theta_{14};\theta_{24};\theta_{34})$ | $N_\tau$ | background |
|---|---|---|---|---|---|
| $(5°;5°;5°;20°)$ | 8.9 | 1.0 | $(10°;5°;5°;20°)$ | 8.5 | 1.0 |
| $(5°;5°;5°;30°)$ | 6.9 | 1.0 | $(10°;5°;5°;30°)$ | 6.5 | 1.0 |
| $(5°;5°;10°;20°)$ | 8.3 | 1.0 | $(10°;5°;10°;20°)$ | 7.9 | 1.0 |
| $(5°;5°;10°;30°)$ | 10.5 | 1.0 | $(10°;5°;10°;30°)$ | 10.3 | 1.0 |
| 3 families | 15.1 | 1.0 | 3 families | 14.4 | 1.0 |

Table 2: *Event rates and expected background for the $\nu_\mu \to \nu_\tau$ channel in the OPERA detector, for different values of $\theta_{14}, \theta_{24}$ and $\theta_{34}$ in the (3+1) scheme. The other unknown angle, $\theta_{13}$ has been fixed to: $\theta_{13} = 5°, 10°$. The CP-violating phases are: $\delta_1 = \delta_2 = 0$; $\delta_3 = 90°$. As a reference, the expected value in the case of standard three-family oscillation (i.e., for $\theta_{i4} = 0$) is shown for maximal CP-violating phase $\delta$. The rates are computed according to Eq.* (15).

according to the allowed regions in the parameter space shown in Sec. 3. The other parameters are: $\theta_{12} = 34°; \theta_{23} = 45°; \Delta m^2_{\rm sol} = 7.9 \times 10^{-5}$ eV$^2$; $\Delta m^2_{\rm atm} = 2.4 \times 10^{-3}$ eV$^2$ and $\Delta m^2_{\rm SBL} = 1$ eV$^2$ (all mass differences are taken to be positive). Eventually, phases have been fixed to: $\delta_1 = \delta_2 = 0; \delta_3 = 90°$. The expected background is also shown. Rates refer to a flux normalized to $4.5 \times 10^{19}$ pot/year (the nominal intensity of the CNGS), an active lead target mass of 1.8 Kton and 5 years of data taking. For comparison, we also report the expected number of events in the usual 3-family scenario.

As it can be seen, in most part of the parameter space we expect a significant depletion of the signal with respect to standard three-neutrino oscillations. However, the difference between (3+1) model $\nu_\mu \to \nu_\tau$ oscillations and standard ones is much bigger than the expected background. A good signal/noise separation can therefore be used to test the model.

### 5.2 $\nu_\mu \to \nu_e$ oscillations

The number of electrons from the $\nu_\mu \to \nu_e$ oscillation is given by the convolution of the $\nu_\mu$ flux $d\phi_{\nu_\mu}(E)/dE$ with the $\nu_e$ charged-current cross-section on lead, $\sigma^{CC}_{\nu_e}(E)$, weighted by the $\nu_\mu \to \nu_e$ oscillation probability, $P_{\mu e}(E)$, times the efficiency for the OPERA detector, $\varepsilon_{\mu e}(E)$ [60]:

$$N_{\mu e} = A \int \frac{d\phi_{\nu_\mu}(E)}{dE} P_{\mu e}(E) \sigma^{CC}_{\nu_e}(E)\, \varepsilon_{\mu e}(E)\, dE\,, \qquad (16)$$

where $A$ is defined as above. The overall signal efficiency $\varepsilon_{\mu e}$ is the convolution of the kinematic efficiency $\varepsilon^{kin}_{\mu e}$ (that ranges from 60% to 80% for neutrino energies between 5 to 20 GeV) and several (nearly factorizable) contributions. Among them, the most relevant are trigger efficiencies, effects due to fiducial volume cuts, vertex and brick finding effi-

| $(\theta_{13};\theta_{14};\theta_{24};\theta_{34})$ | $N_e$ | $\nu_e^{CC}$ | $\nu_\mu^{NC}$ | $\tau \to e$ | $\nu_\mu^{CC}$ |
|---|---|---|---|---|---|
| $(5°;5°;5°;20°)$ | 3.5 | 19.4 | 5.3 | 2.8 | 0.9 |
| $(5°;5°;5°;30°)$ | 3.5 | 19.4 | 5.3 | 2.1 | 0.9 |
| $(5°;5°;10°;20°)$ | 2.4 | 19.4 | 5.3 | 2.3 | 0.9 |
| $(5°;5°;10°;30°)$ | 2.4 | 19.4 | 5.3 | 2.4 | 0.9 |
| 3 families | 3.7 | 19.7 | 5.3 | 4.6 | 0.9 |
| $(10°;5°;5°;20°)$ | 10.6 | 19.4 | 5.3 | 2.7 | 0.9 |
| $(10°;5°;5°;30°)$ | 10.4 | 19.4 | 5.3 | 2.0 | 0.9 |
| $(10°;5°;10°;20°)$ | 8.8 | 19.4 | 5.3 | 2.2 | 0.9 |
| $(10°;5°;10°;30°)$ | 8.6 | 19.4 | 5.3 | 2.4 | 0.9 |
| 3 families | 15.1 | 19.7 | 5.3 | 4.8 | 0.9 |

Table 3: *Event rates and expected background for the $\nu_\mu \to \nu_e$ channel in the OPERA detector, for different values of $\theta_{14}, \theta_{24}$ and $\theta_{34}$ in the (3+1) scheme. The other unknown angle, $\theta_{13}$, has been fixed to: $\theta_{13} = 5°, 10°$. The CP-violating phases are: $\delta_1 = \delta_2 = 0$; $\delta_3 = 90°$. As a reference, the expected value in the case of standard three-family oscillation(i.e., for $\theta_{i4} = 0$) is shown for maximal CP-violating phase $\delta$. The rates are computed according to Eq.* (16)*. Backgrounds have been computed following Ref. [60].*

ciencies and the electron identification capability. They result in a global constant factor $\varepsilon_{\mu e}^{fact} \sim 48\%$.

The dominant sources of background to the $\nu_\mu \to \nu_e$ signal are, in order of importance:

1. $\nu_e$ beam contamination;
2. fake electrons due to $\pi^0$ decays from $\nu_\mu$ NC interactions;
3. electrons produced through $\tau$ decay, where the $\tau$ comes from $\nu_\mu \to \nu_\tau$ oscillations;
4. CC $\nu_\mu$ events where the muon is lost and a track mimics an electron.

Backgrounds (1), (2) and (4) depend very little on the oscillation parameters. On the other hand, the $\tau \to e$ background depends strongly on the active-sterile mixing angles. As we have seen in Sec. 5.1, in the allowed region of the parameter space $\nu_\mu \to \nu_\tau$ oscillations are significantly depleted with respect to the standard three-neutrino ones. As a consequence, this background gets depleted, too.

In Tab. 3 we report the expected number of electrons in the OPERA detector, according to Eq. (16), for different values of $\theta_{13}, \theta_{14}, \theta_{24}$ and $\theta_{34}$. Input points have been chosen according to the allowed regions in the parameter space shown in Sec. 3. The other parameters are: $\theta_{12} = 34°; \theta_{23} = 45°; \Delta m^2_{\text{sol}} = 7.9 \times 10^{-5}$ eV$^2$; $\Delta m^2_{\text{atm}} = 2.4 \times 10^{-3}$ eV$^2$

and $\Delta m^2_{\rm SBL} = 1$ eV$^2$ (all mass differences are taken to be positive). Eventually, phases have been fixed to: $\delta_1 = \delta_2 = 0; \delta_3 = 90^\circ$. Backgrounds have been computed accordingly to Ref. [60]. Rates refer to a flux normalized to $4.5 \times 10^{19}$ pot/year (the nominal intensity of the CNGS), an active lead target mass of 1.8 Kton and 5 years of data taking. For comparison, we also report the expected number of events in the usual 3-family scenario.

As it can be seen from Tab. 3, the difference between the (3+1) model and the standard three-neutrino oscillations are smaller in this channel than in the $\nu_\mu \to \nu_\tau$ one. Moreover, they linearly depends on $\theta_{13}$, as it is clear from Eq. (13). For $\theta_{13} = 5^\circ$, this channel will be of no help to test the allowed parameter space of the (3+1) model. On the other hand, for $\theta_{13}$ saturating the Chooz-Bugey bound, both $\nu_\mu \to \nu_\tau$ and $\nu_\mu \to \nu_e$ might cooperate. However, notice that backgrounds to this signal are much larger than the difference between (3+1) model and standard three-neutrino oscillations for any value of $\theta_{13}$.

## 6 Sensitivity to $(3+1)$ sterile neutrinos at OPERA

In this section we study the sensitivity to $\theta_{13}$ and to the active-sterile mixing angles $\theta_{14}, \theta_{24}$ and $\theta_{34}$ at the CNGS beam, using both the $\nu_\mu \to \nu_\tau$ and $\nu_\mu \to \nu_e$ appearance channels at the OPERA detector. In the rest of this section, the known three-family subspace angles have been fixed to: $\theta_{12} = 34^\circ; \theta_{23} = 45^\circ$. The mass differences have been fixed to: $\Delta m^2_{\rm sol} = 7.9 \times 10^{-5}$ eV$^2$ and $\Delta m^2_{\rm atm} = 2.4 \times 10^{-3}$ eV$^2$. The CP-violating phases $\delta_1$ and $\delta_2$ have been kept fixed to $\delta_1 = \delta_2 = 0$. On the contrary, the CP-violating phase $\delta_3$ is fixed to two values: $\delta_3 = 0$ or $90^\circ$. Notice that this phase is still present in the oscillation probabilities even when $\theta_{12}$ and $\theta_{13}$ vanish, see Eq. (10). At atmospheric $L/E$, oscillations driven by an $\mathcal{O}(\text{eV}^2)$ mass difference are averaged. We have checked that our results apply for any value of $\Delta m^2_{\rm SBL} \geq 0.1$ eV$^2$.

In Fig. 4 we show the sensitivity limit at 99% CL in the $(\theta_{13},\, \theta_{14})$ plane (left) and in the $(\theta_{24},\, \theta_{34})$ plane (right) from a null result of the OPERA experiment, assuming 1, 2, 3, 5 and 10 times the nominal intensity of $4.5 \times 10^{19}$ pot/year. The coloured regions show the present bounds at 90% and 99% CL. We assume $\theta_{23} = 45^\circ$ and $\delta_3 = 0^\circ$ (top) or $\delta_3 = 90^\circ$ (bottom). The sensitivity is defined as the region for which a (poissonian) 2 d.o.f.'s $\chi^2$ is compatible with a "null result" at the 99% CL. We refer to "null result" when $\theta_{13}$ and the three active-sterile mixing angles, $\theta_{14}, \theta_{24}$ and $\theta_{34}$ vanish simultaneously. Both $\nu_\mu \to \nu_\tau$ and $\nu_\mu \to \nu_e$ oscillations have been considered, with the corresponding backgrounds treated properly as in Sec. 5. An overall systematic error of 10% has been taken into account.

In the left panels of Fig. 4 we can see that OPERA can improve only a little the bound on $\theta_{13}$ after 5 years of data taking working at nominal CNGS beam intensity, both for $\delta_3 = 0$ (top panel) or $\delta_3 = 90^\circ$ (bottom panel). Increasing the nominal intensity, however, a significant improvement on the bound is achieved for any value of $\theta_{14}$. Notice that the limit on $\theta_{14}$ is almost unaffected by the OPERA data. This is because for the $\nu_\mu \to \nu_\tau$ and $\nu_\mu \to \nu_e$ oscillation probabilities at atmospheric $L/E$, the $\theta_{14}$-dependence always arises at third-order in the small parameters $\theta_{13}, \theta_{14}, \theta_{24}$ and $\theta_{34}$ (see Eqs. (9) and (10) for the explicit expression in the adopted parametrization, Eq. (3)). On the contrary, the $\theta_{13}$-, $\theta_{24}$- and $\theta_{34}$-dependences in the same oscillation probabilities are quadratic in the small parameters. In case of vanishing active-sterile mixing angles, $\theta_{i4} = 0$, see Ref. [60].

In the right panels of Fig. 4 the sensitivity of OPERA to $\theta_{24}$ and $\theta_{34}$ is shown. First of all, notice that the sensitivity is strongly affected by the intensity of the beam. No improvement on the existing bounds on these two parameters is achieved after 5 years of data taking at nominal CNGS beam intensity, for any of the considered value of $\delta_3$. Already with a doubled flux intensity, some sensitivity to $\theta_{24}, \theta_{34}$ is achievable. The sensitivity enhancement strongly depends on the value of the CP-violating phase $\delta_3$, however. For $\delta_3 = 0$, OPERA can exclude a small part of the 99% CL allowed region, only. On the other hand, for $\delta_3 = 90^\circ$ twice the nominal CNGS flux suffices to put a bound on $\theta_{34} \leq 25^\circ$ for $\theta_{24} \geq 4^\circ$ at 99% CL. For maximal CP-violating $\delta_3$, increasing further the CNGS flux can significantly constrain the $(\theta_{24}, \theta_{34})$ allowed parameter space. Notice, eventually, the strong correlation between $\theta_{24}$ and $\theta_{34}$ in the right panels of Fig. 4. This is an indication that the dominant channel that constrains these angles is $\nu_\mu \to \nu_\tau$. As it can be seen in Eq. (10), the two angles always appear in combination, with an approximate exchange symmetry $\theta_{24} \leftrightarrow \theta_{34}$.

The allowed regions at 99% CL in the $(\theta_{13},\, \theta_{14})$ plane (left) and in the $(\theta_{24},\, \theta_{34})$ plane (right) from the combined analysis of present data and a null result of the OPERA experiment after 5 years of data taking (assuming 1, 2, 3, 5 and 10 times the nominal CNGS intensity of $4.5 \times 10^{19}$ pot/year) are eventually shown in Fig. 5. The coloured regions refer to the present bounds at 90% and 99% CL, for $\theta_{23} = 45^\circ$ and $\delta_3 = 0^\circ$ (top) or $\delta_3 = 90^\circ$ (bottom). As it can be seen, the sensitivity of OPERA strongly benefits from the complementary information on the neutrino parameters provided by other experiments. In this case, even with the nominal beam intensity the extension of the allowed regions is reduced by a moderate but non-negligible amount.

## 7 Conclusions

The results of atmospheric, solar, accelerator and reactor neutrino experiments show that flavour mixing occurs not only in the quark sector, as it has been known for long, but also in the leptonic sector. Experimental data well fit into a three-family scenario. The existence of new "sterile" neutrino states with masses in the eV range is not excluded, however, provided that their couplings with active neutrinos are small enough.

In this paper, we have tried to test the potential of the OPERA experiment at the CNGS beam to improve the present bounds on the parameters of the so-called four-neutrino models. The model, in which only one sterile neutrino is added to the three active ones responsible for solar and atmospheric oscillations, is the minimal extension of the standard three-family oscillation scenario.

We have determined the presently allowed regions for all active-sterile mixing angles and studied the OPERA capability to constrain them further using both the $\nu_\mu \to \nu_e$ and $\nu_\mu \to \nu_\tau$ channels. We have performed our analysis using the OPERA detector as a reference. It can be extended including a detailed simulation of the ICARUS detector at the CNGS beam.

Our conclusions are the following: if the OPERA detector is exposed to the nominal CNGS beam intensity, a null result can improve a bit the present bound on $\theta_{13}$, but not those on the active-sterile mixing angles, $\theta_{14}, \theta_{24}$ and $\theta_{34}$. If the beam intensity is increased by a factor 2 or beyond, not only the sensitivity to $\theta_{13}$ increases accordingly, but a significant sensitivity to $\theta_{24}$ and $\theta_{34}$ is achievable. The $(\theta_{24}, \theta_{34})$ sensitivity strongly depends on the value of the CP-violating phase $\delta_3$, however, with stronger sensitivity for values of $\delta_3$ approaching $\pi/2$. Only a marginal improvement is achievable on the bound on $\theta_{14}$, that should be constrained by high-intensitiy $\nu_e$ disappearance experiments.

Notice that our results hold for any value of $\Delta m^2_{\rm SBL} \geq 0.1$ eV$^2$, *i.e.* in the region of $L/E$ for which oscillations driven by this mass difference are effectively averaged.


## Acknowledgements

We acknowledge E. Fernández-Martínez, P. Hernández, J. López-Pavón, M. Sorel and P. Strolin for useful discussions and comments. We thank T. Schwetz for pointing out to us an error in the first version of the paper and for useful comments on it. The work has been partially supported by the E.U. through the BENE-CARE networking activity MRTN-CT-2004-506395. A.D. received partial support from CiCYT through the project FPA2006-

05423. M.M. received partial support from CiCYT through the project FPA2006-01105 and the MCYT through the *Ramón y Cajal* program. A.D. and M.M. acknowledge also financial support from the Comunidad Autónoma de Madrid through the project P-ESP-00346. D.M. would like to thank CERN, where part of this work has been accomplished.

## References

[1] B. T. Cleveland *et al.*, Astrophys. J. **496** (1998) 505.

[2] J. N. Abdurashitov *et al.* [SAGE Collaboration], Phys. Rev. C **60** (1999) 055801 [arXiv:astro-ph/9907113].

[3] W. Hampel *et al.* [GALLEX Collaboration], Phys. Lett. B **447** (1999) 127.

[4] S. Fukuda *et al.* [Super-Kamiokande Collaboration], Phys. Rev. Lett. **86** (2001) 5651 [arXiv:hep-ex/0103032].

[5] Q. R. Ahmad *et al.* [SNO Collaboration], Phys. Rev. Lett. **87** (2001) 071301 [arXiv:nucl-ex/0106015].

[6] S. N. Ahmed *et al.* [SNO Collaboration], Phys. Rev. Lett. **92** (2004) 181301 [arXiv:nucl-ex/0309004].

[7] Y. Fukuda *et al.* [Super-Kamiokande Collaboration], Phys. Rev. Lett. **81** (1998) 1562 [arXiv:hep-ex/9807003].

[8] M. Ambrosio *et al.* [MACRO Collaboration], Phys. Lett. B **517** (2001) 59 [arXiv:hep-ex/0106049].

[9] M. Apollonio *et al.* [CHOOZ Collaboration], Phys. Lett. B **466** (1999) 415 [arXiv:hep-ex/9907037].

[10] M. Apollonio *et al.* [CHOOZ Collaboration], Eur. Phys. J. C **27** (2003) 331 [arXiv:hep-ex/0301017].

[11] F. Boehm *et al.*, Phys. Rev. D **64** (2001) 112001 [arXiv:hep-ex/0107009].

[12] K. Eguchi *et al.* [KamLAND Collaboration], Phys. Rev. Lett. **90** (2003) 021802 [arXiv:hep-ex/0212021].

[13] M. H. Ahn *et al.* [K2K Collaboration], Phys. Rev. Lett. **90** (2003) 041801 [arXiv:hep-ex/0212007].

[14] E. Aliu *et al.* [K2K Collaboration], Phys. Rev. Lett. **94** (2005) 081802 [arXiv:hep-ex/0411038].

[15] D. G. Michael *et al.* [MINOS Collaboration], Phys. Rev. Lett. **97** (2006) 191801 [arXiv:hep-ex/0607088].

[16] B. Pontecorvo, Sov. Phys. JETP **6** (1957) 429 [Zh. Eksp. Teor. Fiz. **33** (1957) 549].

[17] Z. Maki, M. Nakagawa and S. Sakata, Prog. Theor. Phys. **28** (1962) 870.

[18] B. Pontecorvo, Sov. Phys. JETP **26** (1968) 984 [Zh. Eksp. Teor. Fiz. **53** (1967) 1717].

[19] V. N. Gribov and B. Pontecorvo, Phys. Lett. B **28** (1969) 493.

[20] M. C. Gonzalez-Garcia and M. Maltoni, arXiv:0704.1800 [hep-ph].

[21] C. Athanassopoulos *et al.* [LSND Collaboration], Phys. Rev. C **54** (1996) 2685 [arXiv:nucl-ex/9605001].

[22] C. Athanassopoulos *et al.* [LSND Collaboration], Phys. Rev. Lett. **81** (1998) 1774 [arXiv:nucl-ex/9709006].

[23] A. Aguilar *et al.* [LSND Collaboration], Phys. Rev. D **64** (2001) 112007 [arXiv:hep-ex/0104049].

[24] G. L. Fogli, E. Lisi, A. Marrone and G. Scioscia, arXiv:hep-ph/9906450.

[25] W. M. Yao *et al.* [Particle Data Group], J. Phys. G **33** (2006) 1.

[26] LEP Collaborations (ALEPH, DELPHI, OPAL, L3) *et al.*, Phys. Rept. **427** (2006) 257 [arXiv:hep-ex/0509008].

[27] J. Kleinfeller [KARMEN Collaboration], Nucl. Phys. Proc. Suppl. **87** (2000) 281.

[28] F. Dydak *et al.*, Phys. Lett. B **134** (1984) 281.

[29] I. E. Stockdale *et al.*, Z. Phys. C **27** (1985) 53.

[30] Y. Declais *et al.*, Nucl. Phys. B **434** (1995) 503.

[31] W. Grimus and T. Schwetz, Eur. Phys. J. C **20** (2001) 1 [arXiv:hep-ph/0102252].

[32] S. M. Bilenky, C. Giunti and W. Grimus, Eur. Phys. J. C **1** (1998) 247 [arXiv:hep-ph/9607372].

[33] N. Okada and O. Yasuda, Int. J. Mod. Phys. A **12** (1997) 3669 [arXiv:hep-ph/9606411].

[34] V. D. Barger, S. Pakvasa, T. J. Weiler and K. Whisnant, Phys. Rev. D **58** (1998) 093016 [arXiv:hep-ph/9806328].

[35] S. M. Bilenky, C. Giunti, W. Grimus and T. Schwetz, Phys. Rev. D **60** (1999) 073007 [arXiv:hep-ph/9903454].

[36] O. L. G. Peres and A. Y. Smirnov, Nucl. Phys. B **599** (2001) 3 [arXiv:hep-ph/0011054].

[37] C. Giunti and M. Laveder, JHEP **0102** (2001) 001 [arXiv:hep-ph/0010009].

[38] M. Maltoni, T. Schwetz, M. A. Tortola and J. W. F. Valle, New J. Phys. **6** (2004) 122 [arXiv:hep-ph/0405172].

[39] M. Maltoni, T. Schwetz, M. A. Tortola and J. W. F. Valle, Nucl. Phys. B **643** (2002) 321 [arXiv:hep-ph/0207157].

[40] M. Sorel, J. M. Conrad and M. Shaevitz, Phys. Rev. D **70** (2004) 073004 [arXiv:hep-ph/0305255].

[41] E. D. Church, K. Eitel, G. B. Mills and M. Steidl, Phys. Rev. D **66** (2002) 013001 [arXiv:hep-ex/0203023].

[42] A. A. Aguilar-Arevalo *et al.* [The MiniBooNE Collaboration], Phys. Rev. Lett. **98** (2007) 231801 [arXiv:0704.1500 [hep-ex]].

[43] M. Maltoni and T. Schwetz, arXiv:0705.0107 [hep-ph], to appear in PRD.

[44] A. de Gouvea, Phys. Rev. D **72** (2005) 033005 [arXiv:hep-ph/0501039].

[45] A. de Gouvea, J. Jenkins and N. Vasudevan, Phys. Rev. D **75** (2007) 013003 [arXiv:hep-ph/0608147].

[46] S. Palomares-Ruiz, S. Pascoli and T. Schwetz, JHEP **0509** (2005) 048 [arXiv:hep-ph/0505216].

[47] H. Pas, S. Pakvasa and T. J. Weiler, Phys. Rev. D **72** (2005) 095017 [arXiv:hep-ph/0504096].

[48] G. Giacomelli, arXiv:physics/0703247.

[49] R. Acquafredda *et al.* [OPERA Collaboration], New J. Phys. **8** (2006) 303 [arXiv:hep-ex/0611023].

[50] S. Amerio *et al.* [ICARUS Collaboration], Nucl. Instrum. Meth. A **527** (2004) 329.

[51] A. Donini and D. Meloni, Eur. Phys. J. C **22** (2001) 179 [arXiv:hep-ph/0105089].

[52] A. Donini, M. Lusignoli and D. Meloni, Nucl. Phys. B **624** (2002) 405 [arXiv:hep-ph/0107231].

[53] M. Maltoni, T. Schwetz, M. A. Tortola and J. W. F. Valle, Phys. Rev. D **67** (2003) 013011 [arXiv:hep-ph/0207227].

[54] S. M. Bilenky, S. Pascoli and S. T. Petcov, Phys. Rev. D **64** (2001) 113003 [arXiv:hep-ph/0104218].

[55] A. Donini, M. B. Gavela, P. Hernandez and S. Rigolin, Nucl. Phys. B **574** (2000) 23 [arXiv:hep-ph/9909254].

[56] A. Donini, M. B. Gavela, P. Hernandez and S. Rigolin, Nucl. Instrum. Meth. A **451** (2000) 58 [arXiv:hep-ph/9910516].

[57] A. De Rujula, M. Lusignoli, L. Maiani, S. T. Petcov and R. Petronzio, Nucl. Phys. B **168** (1980) 54.

[58] A.E. Ball *et al.*, "CNGS: Update on secondary beam layout", SL-Note-2000-063 EA.

[59] P. Migliozzi, Nucl. Phys. Proc. Suppl. **155** (2006) 23.

[60] M. Komatsu, P. Migliozzi and F. Terranova, J. Phys. G **29** (2003) 443 [arXiv:hep-ph/0210043].

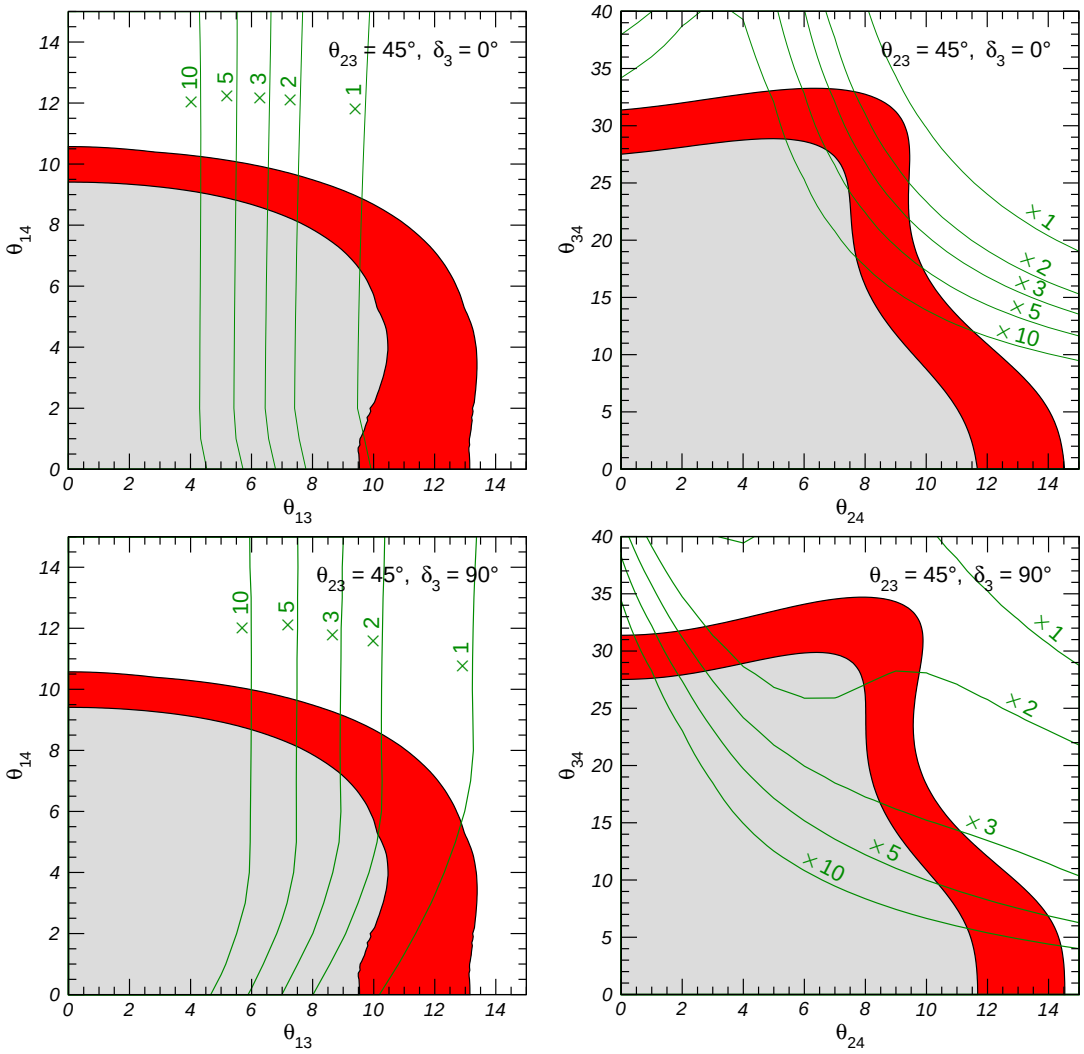


Figure 4: *Sensitivity limit at 99% CL in the* $(\theta_{13}, \theta_{14})$ *plane (left) and in the* $(\theta_{24}, \theta_{34})$ *plane (right) from a null result of the OPERA experiment, assuming 1, 2, 3, 5 and 10 times the nominal intensity of* $4.5 \times 10^{19}$ *pot/year. The coloured regions show the present bounds at 90% and 99% CL. We assume* $\theta_{23} = 45°$ *and* $\delta_3 = 0°$ *(top) or* $\delta_3 = 90°$ *(bottom).*

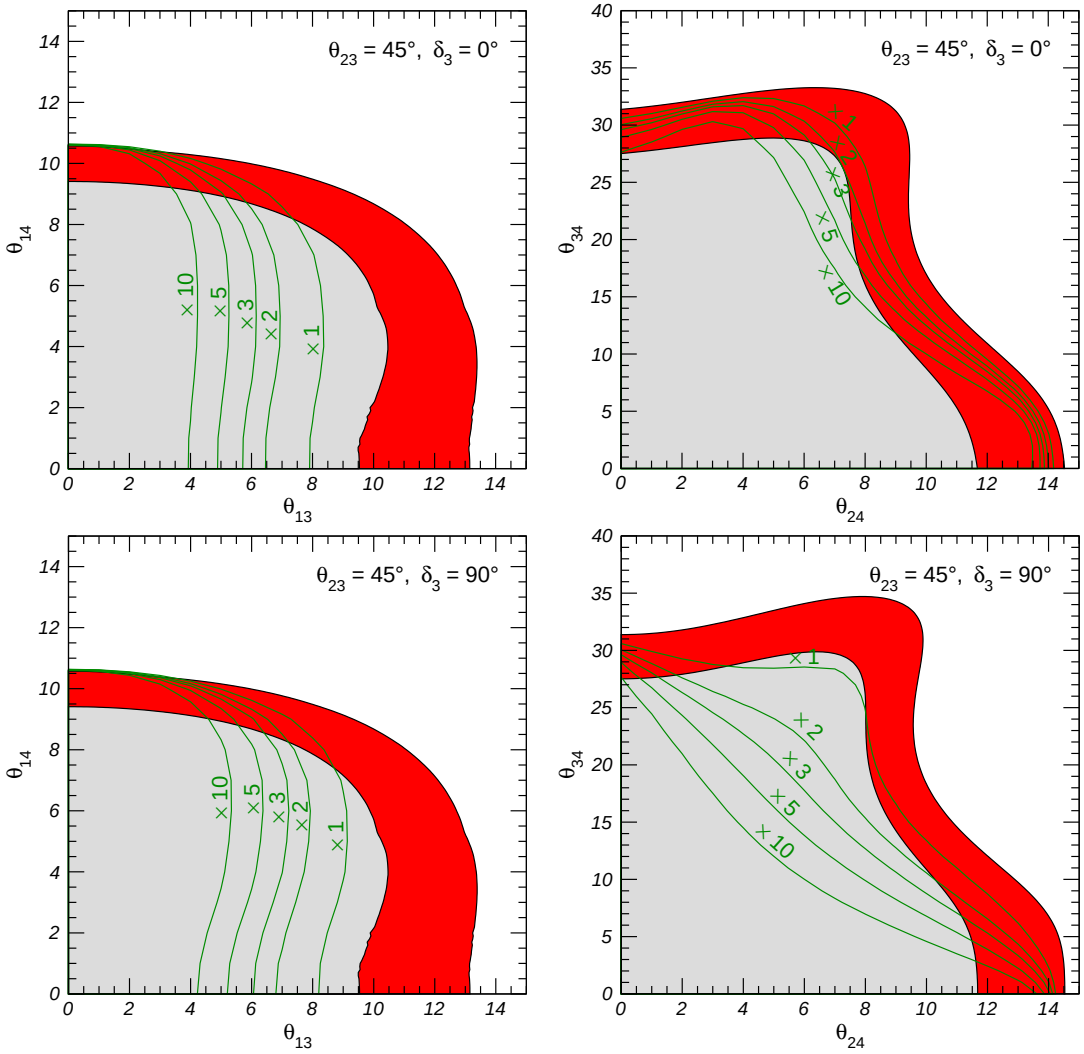


Figure 5: *Sensitivity limit at 99% CL in the* $(\theta_{13}, \theta_{14})$ *plane (left) and in the* $(\theta_{24}, \theta_{34})$ *plane (right) from the combined analysis of present data and a null result of the OPERA experiment, assuming 1, 2, 3, 5 and 10 times the nominal intensity of* $4.5 \times 10^{19}$ *pot/year. The coloured regions show the present bounds at 90% and 99% CL. We assume* $\theta_{23} = 45^\circ$ *and* $\delta_3 = 0^\circ$ *(top) or* $\delta_3 = 90^\circ$ *(bottom).*